Available online at www.sciencedirect.com
SCIENCE DIRECT
Journal of Sound and Vibration 294 (2006) 486–502
JOURNAL OF SOUND AND VIBRATION
www.elsevier.com/locate/jsvi

# Variation in the stability of a rotating blade disk with a local crack defect

Bo-Wun Huang[a], Jao-Hwa Kuang[b,*]

[a]Department of Mechanical Engineering, Cheng Shiu University, Kaohsiung, Taiwan, ROC
[b]Department of Mechanical and Electromechanical Engineering, National Sun Yat-Sen University, Kaohsiung, Taiwan, ROC

Received 1 February 2005; accepted 19 November 2005
Available online 17 February 2006

**Abstract**

The effect of a near root local blade crack on the stability of a grouped blade disk is investigated in this paper. A bladed disk comprised of periodically shrouded blades is used to simulate the coupled periodic structure. The blade crack is modeled using the local flexibility with coupling terms. The mode localization phenomenon introduced by the blade crack on the longitudinal and bending vibrations in the rotating blades has also been considered. Using the Galerkin's method, the imperturbation equations of a bladed disk in which one of the blades is cracked, subject to fluctuations in the rotation speed, can be derived. Employing the multiple scales method, the boundaries of the instability zones in the mistuned turbo blade system are approximated. Numerical results indicate that an additional unstable zone is introduced near the localization frequency and the regions of unstable zones are varied with the crack size and fluctuations in disk speed.


## 1. Introduction

The local structural or material irregularities or defects in a periodic blade-disk system may introduce the so-called localization phenomenon. The fluctuation energy will be confined in those blades near the disordered blade. In the last decade, a number of studies were conducted to investigate mode localization in periodic structures [1–5]. Recently, Cai et al. [6,7] studied mode localization in nearly periodic systems in one, two and three dimensions. Generally, a periodically shrouded blade disk of a turbo rotor can be regarded as a typical periodic system. The vibration in a shrouded blade disk was first discussed by Cottney and Ewins [8]. Due to manufacturing flaws or cyclic fatigue, numerous cracks might be observed after severe operation [9,10]. The fundamental aspects of the dynamic problem in a system with a local defect were studied by Afolabi et al. [11–14].

During actual service, the rotation speed of a shrouded blade disk will not always remain constant. The blade disk is subjected to some small fluctuations. Theoretically, at some specified rotation speed, this

*Corresponding author. Department of Mechanical Engineering, National Sun Yat-Sen University, Kaohsiung, Taiwan, ROC. Tel.: +886 7 525 2000; fax: +886 7 525 4299.
*E-mail address:* kuang@mail.nsysu.edu.tw (J.-H. Kuang).

0022-460X/$ - see front matter © 2006 Elsevier Ltd. All rights reserved.
doi:10.1016/j.jsv.2005.11.028

**Nomenclature**

| | |
|---|---|
| $A$ | cross section area of the blade |
| $a$ | depth of crack |
| $b$ | width of the blade |
| $c.c.$ | complex conjugate of the preceding term |
| $E$ | Young's modulus of material of blade |
| $F(t)$ | the varying rotating speed |
| $s$ | the number of blade |
| $I$ | moment of inertia |
| $k_s$ | the stiffness |
| $L$ | length of cantilever beam |
| $N$ | total number of blades |
| $\{p\}_s\{q\}_s$ | displacement vectors of the radial and transverse directions of $s$th blade |
| $p_i^s(t)q_i^s(t)$ | determined coefficient for radial and transverse direction for the $s$th blade, $i = 1, 2, \ldots, 5$ |
| $R_c$ | position of coupled spring |
| $R_h R_o$ | inner and outer diameter of disk |
| $r$ | arbitrary position on the blade |
| $\bar{r}^*$ | dimensionless cracked position on the blade |
| $t$ | thickness of the blade |
| $u_s(r,t)$ | deflection in radial direction of the $s$th blade |
| $v_s(r,t)$ | deflection in transverse direction of the $s$th blade |
| $\bar{\beta}$ | dimensionless stiffness |
| $\bar{\theta}_j$ | perturbation frequency |
| $\varepsilon$ | perturbation parameter |
| $\lambda_i$ | coefficient |
| $\rho$ | density of blade |
| $\sigma_i$ | coefficient |
| $\phi_i(\bar{r})\psi_i(\bar{r})$ | comparison functions |
| $\Omega$ | rotation speed |
| $\Omega_0$ | the steady-state rotating speed |
| $\bar{\omega}$ | excitating frequency on the system |
| $\bar{\omega}_1^*$ | the lowest natural frequency of the tuned system |
| $\bar{\omega}_n$ | natural frequency of the mistuned system |

small speed fluctuation may drive the system into a dynamically unstable condition. Most of the studies on the stability of a bladed disk system focused on the speed fluctuation effect [15–18]. Only a few studies, such as [19], on the flutter stability in mistuned systems, have been conducted. As noted in many papers, a local defect in a periodical structure may alter its dynamic characteristics and introduce so-called localization modes in the mistuned periodical system. The stability characteristics of a mistuned blade disk with a crack is worthy of attention, because local structural or material defects in a blade-disk system are unavoidable.

In this work, the effect of the localization modes on the dynamic instability of a periodically shrouded blade disk is studied. A small fluctuation superimposed on a steady rotational speed is assumed to characterize a disturbed rotational speed. For simplicity, the blades are approximated as Euler–Bernoulli beams. The Galerkin method and the multiple scales perturbation method are used to determine the boundaries of instability in this mistuned system. The Coriolis force, coupled vibration, crack size, shrouded stiffness, and rotation speed effects on the instability in the mistuned blade disk are investigated in this study.

## 2. Equations of motion

A periodic, shrouded blade disk is shown in Fig. 1(a). The disk system is composed of a rigid hub and a cyclic assembly of $N$ coupled blades, where an individual blade is modeled simply as a cantilever Euler–Bernoulli beam. Each blade is coupled with the adjacent blade through a shroud. The length of each cantilever beam is $L = R_o - R_h$. Consider that, every blade is coupled by a massless spring $k_s$ with the adjacent blade at position $R_c$. The notations $u_s(r,t)$ and $v_s(r,t)$ denote the radial and the transverse flexible deflections of the $s$th blade with a rotation speed of $\Omega$. The moment of inertia and the cross sectional area of the $s$th blade are denoted as $I$ and $A$. The inertia of the cross sectional area is $I = bt^3/12$. $b$ and $t$ are the width and height of the blade, respectively. $E$ is the Young's modulus of the blade. The equations of motion for blades with and without a crack are derived in the following sections.

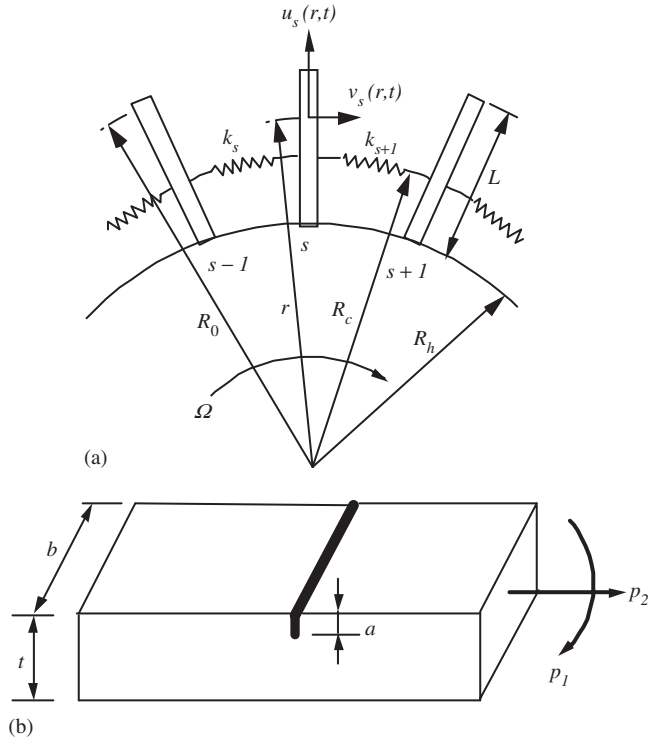


Fig. 1. Geometry of the shrouded blade disk.

### 2.1. Blades without crack

Considering the Coriolis force effect [20,21], the equations of motion of the $s$th blade in the radial and transverse directions are displayed [22]. In this article, the rotational speed is assumed to fluctuate with a small perturbation speed $f(t)$.

$$\Omega(t) = \Omega_0 + f(t). \tag{1}$$

If the constant speed $\Omega_0$ is much smaller than the first natural frequency of the blade [15,23], the centrifugal force $F_c$ may be assumed to be constant and displayed as

$$F_c = \tfrac{1}{2}\rho A\Omega_0^2[(R_h + L)^2 - r^2]. \tag{2}$$

The non-dimensional equations of motion for the $s$th blade in the radial and transverse directions can then be displayed as

$$\ddot{\bar{u}}_s - \alpha(2\bar{\Omega}_0\dot{\bar{v}}_s) - \alpha^2\left[\bar{\Omega}_0^2\bar{u}_s + \frac{AL^2}{I}(\bar{u}_s')'\right] = 2\alpha\bar{f}\,\dot{\bar{v}}_s + \alpha^2(2\bar{\Omega}_0\bar{f} + \bar{f}^2)\bar{u}_s, \tag{3a}$$

$$\ddot{\bar{v}}_s + \alpha(2\bar{\Omega}_0\dot{\bar{u}}_s) + \alpha^2\bar{\Omega}_0^2\left\{\bar{r}\bar{v}_s' - \bar{v}_s - \frac{1}{2}\left[\left(\frac{R_h}{L} + 1\right)^2 - \bar{r}^2\right]\bar{v}_s''\right\} + \alpha^2(\bar{v}_s'')'' + (\bar{\beta}_{s+1} + \bar{\beta}_s)\bar{v}_s\delta(\bar{r} - \bar{R}_c)$$
$$- \bar{\beta}_{s+1}\bar{v}_{s+1}\delta(\bar{r} - \bar{R}_c) - \bar{\beta}_s\bar{v}_{s-1}\delta(\bar{r} - \bar{R}_c) = -2\alpha\bar{f}\,\dot{\bar{u}}_s + \alpha^2(2\bar{\Omega}_0\bar{f} + \bar{f}^2)\bar{v}_s, \tag{3b}$$

where $\alpha = \sqrt{EI/\rho AL^4}$. for $s = 1, 2, \ldots, N$. The corresponding boundary conditions are

$$\bar{u}_s = \bar{v}_s = \bar{v}_s' = 0 \quad \text{at } \bar{r} = 0, \tag{4a}$$

$$\bar{u}_s' = \bar{v}_s'' = \bar{v}_s''' = 0 \quad \text{at } \bar{r} = 1. \tag{4b}$$

The non-dimensional parameters are defined as

$$\bar{r} = \frac{r - R_h}{L} \quad \text{and} \quad \bar{r} = 0 \text{ to } 1, \tag{5a}$$

$$\bar{v}_s(\bar{r}, t) = \frac{v_s(\bar{r}, t)}{L}, \quad \bar{u}_s(\bar{r}, t) = \frac{u_s(\bar{r}, t)}{L}, \tag{5b}$$

$$\bar{\Omega}_0 = \Omega_0 \Big/ \sqrt{\frac{EI}{\rho A L^4}}, \tag{5c}$$

$$\bar{R}_c = \frac{R_c - R_h}{L}, \tag{5d}$$

$$\bar{\beta}_s = \frac{k_s L^3}{EI_s}, \tag{5e}$$

$$\bar{f} = f \Big/ \sqrt{\frac{EI}{\rho A L^4}}. \tag{5f}$$

The solutions for the above eigenvalue problem are expressed as

$$\bar{u}_s(\bar{r}, t) = \sum_{i=1}^{m} p_i^s(t)\phi_i^s(\bar{r}), \tag{6a}$$

$$\bar{v}_s(\bar{r}, t) = \sum_{i=1}^{m} q_i^s(t)\psi_i^s(\bar{r}), \tag{6b}$$

where $\phi_i^s(\bar{r})$, $\psi_i^s(\bar{r})$ are the comparison functions for Eqs. (3a) and (3b), and $p_i^s(t), q_i^s(t)$ are the corresponding weighting coefficients, which are to be determined. Six exact solutions for a uniform cantilever beam, i.e., three tensile modes $\phi_i^s(\bar{r})$ in the axial direction and three bending modes $\psi_i^s(\bar{r})$ in the transverse direction are used in this study. They are

$$\phi_i^s(\bar{r}) = \sin\, \sigma_i \bar{r}, \tag{7a}$$

$$\psi_i^s(\bar{r}) = (\cosh\, \lambda_i \bar{r} - \cos\, \lambda_i \bar{r}) - \frac{\cos\, \lambda_i + \cosh\, \lambda_i}{\sin\, \lambda_i + \sinh\, \lambda_i}(\sinh\, \lambda_i \bar{r} - \sin\, \lambda_i \bar{r}) \quad \text{for } i = 1, 2, \ldots, m. \tag{7b}$$

By applying Galerkin's method, Eqs. 3(a) and 3(b) can be rewritten in the matrix form as

$$[m_1]_s\{\ddot{p}\}_s + \alpha[g_1]_s\{\dot{q}\}_s + \alpha^2([k_1]_s + [\Lambda_1]_s)\{p\}_s = 2\alpha\bar{f}[d_1]_s\{\dot{q}\}_s + \alpha^2(2\bar{\Omega}_0\bar{f} + \bar{f}^2)[e_1]_s\{p\}_s, \tag{8a}$$

$$\begin{aligned}&[m_2]_s\{\ddot{q}\}_s + \alpha[g_2]_s\{\dot{p}\}_s + \alpha^2\{[[k_2]_s + [\Lambda_2]_s + \bar{\beta}_{s+1}\{\psi(\bar{R}_c)\}_s\{\psi(\bar{R}_c)\}_s^{\mathrm{T}} + \bar{\beta}_s\{\psi(\bar{R}_c)\}_s\{\psi(\bar{R}_c)\}_s^{\mathrm{T}}]\{q\}_s\\ &\quad - \bar{\beta}_s\{\psi(\bar{R}_c)\}_s\{\psi(\bar{R}_c)\}_{s-1}^{\mathrm{T}}\{q\}_{s-1} - \bar{\beta}_{s+1}\{\psi(\bar{R}_c)\}_s\{\psi(\bar{R}_c)\}_{s+1}^{\mathrm{T}}\{q\}_{s+1}\} = -2\alpha\bar{f}[d_2]_s\{\dot{p}\}_s + \alpha^2(2\bar{\Omega}_0\bar{f} + \bar{f}^2)[e_2]_s\{q\}_s\\ &\text{for } s = 1, 2, \ldots, N \quad \text{and} \quad \{\psi\}_s = [\psi_1^s, \psi_2^s, \psi_3^s, \ldots, \psi_m^s]^{\mathrm{T}}.\end{aligned} \tag{8b}$$

Due to the cyclic arrangement of blade, it leads to

$$\{p\}_{N+1} = \{p\}_1, \{q\}_{N+1} = \{q\}_1.$$

For simplicity, the same comparison function is assumed for individual blades, i.e., $\phi_j^s(\bar{r}) \equiv \phi_j(\bar{r}), \psi_j^s(\bar{r}) \equiv \psi_j(\bar{r})$. Combining the above two equations for the $s$th blade, yields

$$[m]_s \begin{Bmatrix} \ddot{p} \\ \ddot{q} \end{Bmatrix}_s + \alpha[g]_s \begin{Bmatrix} \dot{p} \\ \dot{q} \end{Bmatrix}_s + \alpha^2 \left\{ [[k]_s + [\Lambda]_s + \bar{\beta}_{s+1}[\Phi] + \bar{\beta}_s[\Phi]] \begin{Bmatrix} p \\ q \end{Bmatrix}_s - \bar{\beta}_s[\Phi] \begin{Bmatrix} p \\ q \end{Bmatrix}_{s-1} - \bar{\beta}_{s+1}[\Phi] \begin{Bmatrix} p \\ q \end{Bmatrix}_{s+1} \right\}$$
$$= 2\alpha\bar{f}[d]_s \begin{Bmatrix} \dot{p} \\ \dot{q} \end{Bmatrix}_s + \alpha^2(2\bar{\Omega}_0\bar{f} + \bar{f}^2)[e]_s \begin{Bmatrix} p \\ q \end{Bmatrix}_s. \tag{9}$$

### 2.2. Blade with a crack

A number of researchers [24–26] have studied the effect of cracks on the dynamic and static structural behaviors. Some articles from Refs. [27–30] also dealt with the effect of cracks on rotating machinery. More recent articles like Refs. [31–34] investigate the stability of a rotating blade without or with a crack. No investigation studies the stability on mode localization in a rotating periodic blades system. The cracked shrouded blade disk may be regarded as a mistuned system. Consider a crack located at $\bar{r} = \bar{r}^*$ on the $\xi$th blade. The strain energy of the defective blade will consist of the released energy caused by the crack. The released energy caused by a crack with a depth of $a$ may be expressed as

$$U_\xi^c = b \int_0^a \frac{(1-\mu^2)}{E} K_I^2 \, \mathrm{d}a, \tag{10}$$

where $\mu$ is the Poisson's ratio of the blade, and $K_I$ is the stress intensity factor under a mode $I$ load. As noted in Ref. [24], this stress intensity factor $K_I$ will be considered as $K_I = K_{I1} + K_{I2}$, if the deflection is coupled from the longitudinal and bending deformations. In this case, the stress intensity factors $K_{I1}$ and $K_{I2}$ can be approximated by [25] as

$$K_{I1} = \frac{6p_1}{t^2 b} \sqrt{\pi\bar{\gamma}t} F_{I1}(\bar{\gamma}), \tag{11a}$$

$$K_{I2} = \frac{p_2}{tb} \sqrt{\pi\bar{\gamma}t} F_{I2}(\bar{\gamma}) \tag{11b}$$

with

$$p_1 = EIv''_\xi|_{\bar{r}=\bar{r}^*}, \tag{12a}$$

$$p_2 = EAu'_\xi|_{\bar{r}=\bar{r}^*}, \tag{12b}$$

$$\bar{\gamma} = \frac{a}{t}, \tag{13}$$

$$F_{I1}(\bar{\gamma}) = \sqrt{\frac{2}{\pi\bar{\gamma}} \tan\left(\frac{\pi\bar{\gamma}}{2}\right)} \frac{0.923 + 0.199[1 - \sin(\pi\bar{\gamma}/2)]^4}{\cos(\pi\bar{\gamma}/2)}, \tag{14a}$$

$$F_{I2}(\bar{\gamma}) = \sqrt{\frac{2}{\pi\bar{\gamma}} \tan(\pi\bar{\gamma}/2)} \frac{0.752 + 2.02(\bar{\gamma}) + 0.37[1 - \sin(\pi\bar{\gamma}/2)]^3}{\cos(\pi\bar{\gamma}/2)}. \tag{14b}$$

Adapting Eq. (10) gives

$$U_\xi^c = b\frac{(1-\mu^2)}{E} \int_0^a \left\{ \left[ \frac{6EIv''_\xi \delta(\bar{r} - \bar{r}^*)}{t^2 b} \sqrt{\pi\bar{\gamma}t} F_{I1}(\bar{\gamma}) \right]^2 + 2 \left[ \frac{6EIv''_\xi \delta(\bar{r} - \bar{r}^*)}{t^2 b} \sqrt{\pi\bar{\gamma}t} F_{I1}(\bar{\gamma}) \right] \right.$$
$$\left. \times \left[ \frac{EAu'_\xi \delta(\bar{r} - \bar{r}^*)}{tb} \sqrt{\pi\bar{\gamma}t} F_{I2}(\bar{\gamma}) \right] + \left[ \frac{EAu'_\xi \delta(\bar{r} - \bar{r}^*)}{tb} \sqrt{\pi\bar{\gamma}t} F_{I2}(\bar{\gamma}) \right]^2 \right\} \mathrm{d}a. \tag{15}$$

The boundary conditions of the defective blade are the same as that for the $s$th blade, i.e., the blade without a crack. Therefore, the equations of motion for the $\xi$th cracked blade can be derived as follows:

$$\ddot{\bar{u}}_\xi - \alpha(2\bar{\Omega}_0\dot{\bar{v}}_\xi) - \alpha^2\left[\bar{\Omega}_0^2\bar{u}_\xi + \frac{AL^2}{I}(\bar{u}'_\xi)'\right] + \alpha^2\left\{\left[24\frac{L}{t}(1-\mu^2)Q_3(\bar{\gamma})[\bar{u}'_\xi\delta(\bar{r}-\bar{r}^*)]\right]'[12(1-\mu^2)Q_2(\bar{\gamma})[\bar{v}''_\xi\delta(\bar{r}-\bar{r}^*)]]\right\}$$
$$= 2\alpha\bar{f}\,\dot{\bar{v}}_\xi + \alpha^2(2\bar{\Omega}_0\bar{f}+\bar{f}^2)\bar{u}_\xi, \tag{16a}$$

$$\ddot{\bar{v}}_\xi + \alpha(2\bar{\Omega}_0\dot{\bar{u}}_\xi) + \alpha^2\bar{\Omega}_0^2\left\{\bar{r}\bar{v}'_\xi - \bar{v}_\xi - \frac{1}{2}\left[\left(\frac{R_h}{L}+1\right)^2 - \bar{r}^2\right]\bar{v}''_\xi\right\} + \alpha^2(\bar{v}''_\xi)''$$
$$- \alpha^2\left\{[12(1-\mu^2)Q_2(\bar{\gamma})[\bar{u}'_\xi\delta(\bar{r}-\bar{r}^*)]''] + 6(1-\mu^2)\frac{t}{L}Q_1(\bar{\gamma})[\bar{v}''_\xi\delta(\bar{r}-\bar{r}^*)]''\right\}$$
$$+ (\bar{\beta}_{\xi+1}+\bar{\beta}_\xi)\bar{v}_\xi\delta(\bar{r}-\bar{R}_c) - \bar{\beta}_{\xi+1}\bar{v}_{\xi+1}\delta(\bar{r}-\bar{R}_c) - \bar{\beta}_\xi\bar{v}_{\xi-1}\delta(\bar{r}-\bar{R}_c) = -2\alpha\bar{f}\,\dot{\bar{u}}_\xi + \alpha^2(2\Omega_0\bar{f}+\bar{f}^2)\bar{v}_\xi, \tag{16b}$$

where

$$Q_1(\bar{\gamma}) = \int_0^{\bar{\gamma}} \pi\bar{\gamma}F_{I1}^2(\bar{\gamma})\,\mathrm{d}\bar{\gamma}, \tag{17a}$$

$$Q_2(\bar{\gamma}) = \int_0^{\bar{\gamma}} \pi\bar{\gamma}F_{I1}(\bar{\gamma})F_{I2}(\bar{\gamma})\,\mathrm{d}\bar{\gamma}, \tag{17b}$$

$$Q_3(\bar{\gamma}) = \int_0^{\bar{\gamma}} \pi\bar{\gamma}F_{I2}^2(\bar{\gamma})\,\mathrm{d}\bar{\gamma}. \tag{17c}$$

The boundary conditions for the $\xi$th cracked blade are the same as Eqs. 4(a) and 4(b). Similarly, the equations of motion for the defective blade, i.e., Eqs. 16(a) and 16(b), can also be rearranged in the matrix form using Galerkin's method.

### 2.3. Total blade-disk system

The equation of motion for the assembled blade-disk system can now be given by

$$[M]\{\ddot{X}\} + \alpha[G]\{\dot{X}\} + \alpha^2[K]\{X\} = 2\alpha\bar{f}[D]\{\dot{X}\} + \alpha^2(2\bar{\Omega}_0\bar{f}+\bar{f}^2)[E]\{X\}, \tag{18}$$

where the system stiffness matrix $[K]$ is

$$[K] = \begin{bmatrix} [\bar{\eta}]_1 & -\bar{\beta}_2[\Phi] & 0 & \cdot & 0 & 0 & -\bar{\beta}_1[\Phi] \\ -\bar{\beta}_2[\Phi] & [\bar{\eta}]_2 & -\bar{\beta}_3[\Phi] & \cdot & 0 & 0 & 0 \\ 0 & -\bar{\beta}_3[\Phi] & [\bar{\eta}]_3 & \cdot & 0 & 0 & 0 \\ \cdot & \cdot & \cdot & \cdot & \cdot & \cdot & \cdot \\ 0 & 0 & 0 & \cdot & [\bar{\eta}]_{N-2} & -\bar{\beta}_{N-1}[\Phi] & 0 \\ 0 & 0 & 0 & \cdot & -\bar{\beta}_{N-1}[\Phi] & [\bar{\eta}]_{N-1} & -\bar{\beta}_N[\Phi] \\ -\bar{\beta}_1[\Phi] & 0 & 0 & \cdot & 0 & -\bar{\beta}_N[\Phi] & [\bar{\eta}s]_N \end{bmatrix}. \tag{19}$$

The displacement vector is

$$\{X\} = \left[\{x\}_1^{\mathrm{T}}, \{x\}_2^{\mathrm{T}}, \ldots, \{x\}_{N-1}^{\mathrm{T}}, \{x\}_N^{\mathrm{T}}\right]^{\mathrm{T}} \tag{20}$$

and

$$\{x\}_s = \begin{Bmatrix} p \\ q \end{Bmatrix}_s,$$

$$[\bar{\eta}]_s = [k]_s + [\Lambda]_s + \bar{\beta}_{s+1}[\Phi] + \bar{\beta}_s[\Phi], \tag{21}$$

$$\bar{\beta}_1 = \bar{\beta}_{N+1}. \tag{22}$$

For solving the eigenvalue problem of the system, i.e., Eq. (18), a space vector is introduced

$$\{V\} = \begin{Bmatrix} \dot{X} \\ X \end{Bmatrix}. \tag{23}$$

Substituting Eq. (23) into Eq. (18), the equation can be rearranged as

$$\begin{bmatrix} [M] & 0 \\ 0 & \alpha^2[K] \end{bmatrix}\{\dot{V}\} + \begin{bmatrix} \alpha[G] & \alpha^2[K] \\ -\alpha^2[K] & 0 \end{bmatrix}\{V\} = 2\bar{f}\begin{bmatrix} \alpha[D] & 0 \\ 0 & 0 \end{bmatrix}\{V\} + (2\bar{\Omega}_0\bar{f} + f^2)\begin{bmatrix} 0 & \alpha^2[E] \\ 0 & 0 \end{bmatrix}\{V\}. \tag{24}$$

The non-dimensional frequencies $\bar{\omega}_n$ in Eq. (24), i.e., the natural frequencies of the mistuned system, are defined as

$$\bar{\omega}_n = \omega_n \Big/ \sqrt{\frac{EI}{\rho A L^4}} \quad \text{for} \quad n = 1, 2, \ldots. \tag{25}$$

## 3. Perturbation analysis

Eq. (24) is a set of simultaneous differential equations, which are difficult to solve directly. To make the calculation easier, modal analysis application is employed here. After applying the modal analysis method, the simultaneous differential equation, can be rewritten as

$$[I]\{\dot{u}\} + [A]\{u\} = -2\frac{\bar{f}}{\bar{\Omega}_0}[S]\{u\} - \left(\frac{2\bar{f}}{\bar{\Omega}_0} + \frac{\bar{f}^2}{\bar{\Omega}_0^2}\right)[Q]\{u\} \tag{26}$$

with

$$[\Delta]^{\mathrm{T}}\begin{bmatrix} [M] & 0 \\ 0 & \alpha^2[K] \end{bmatrix}[\Delta] = [I] = \begin{bmatrix} 1 & 0 & 0 & \cdots & 0 \\ 0 & 1 & 0 & \cdots & 0 \\ \vdots & & \ddots & & \vdots \\ 0 & 0 & 0 & & 1 \end{bmatrix}, \tag{27a}$$

$$[\Delta]^{\mathrm{T}}\begin{bmatrix} \alpha[G] & \alpha^2[K] \\ -\alpha^2[K] & 0 \end{bmatrix}[\Delta] = [A], \tag{27b}$$

$$-\bar{\Omega}_0[\Delta]^{\mathrm{T}}\begin{bmatrix} \alpha[D] & 0 \\ 0 & 0 \end{bmatrix}[\Delta] = [S], \tag{27c}$$

$$-\bar{\Omega}_0^2[\Delta]^{\mathrm{T}}\begin{bmatrix} 0 & \alpha^2[E] \\ 0 & 0 \end{bmatrix}[\Delta] = [Q], \tag{27d}$$

$$\{V\} = [\Delta]\{u\}. \tag{27e}$$

The normalized modal matrix $[\Delta]$ is comprised of $m$ modes from Eq. (24) with no perturbation terms. The block diagonal matrix $[A]$ is

$$[A]=\begin{bmatrix} \begin{bmatrix} 0 & -\bar{\omega}_1 \\ \bar{\omega}_1 & 0 \end{bmatrix} & [0] & [0] & [0] & [0] & [0] \\ [0] & \begin{bmatrix} 0 & -\bar{\omega}_2 \\ \bar{\omega}_2 & 0 \end{bmatrix} & [0] & [0] & [0] & [0] \\ \cdot & \cdot & \cdot & & & \cdot \\ \cdot & \cdot & & \cdot & & \cdot \\ \cdot & \cdot & & & \cdot & \cdot \\ [0] & [0] & \cdot & \cdot & [0] & \begin{bmatrix} 0 & -\bar{\omega}_m \\ \bar{\omega}_m & 0 \end{bmatrix} \end{bmatrix}. \tag{28}$$

Eq. (26) can then be uncoupled, and displayed in the component form as

$$\dot{\varsigma}_n-\bar{\omega}_n\eta_n=-2\frac{\bar{f}}{\bar{\Omega}_0}\left(\sum_{r=1}^{R}S_{nr}^{11}\zeta_r+\sum_{r=1}^{R}S_{nr}^{12}\eta_r\right)-\left(2\frac{\bar{f}}{\bar{\Omega}_0}+\frac{\bar{f}^2}{\bar{\Omega}_0^2}\right)\left(\sum_{r=1}^{R}Q_{nr}^{11}\zeta_r+\sum_{r=1}^{R}Q_{nr}^{12}\eta_r\right), \tag{29a}$$

$$\dot{\eta}_n+\bar{\omega}_n\varsigma_n=-2\frac{\bar{f}}{\bar{\Omega}_0}\left(\sum_{r=1}^{R}S_{nr}^{21}\zeta_r+\sum_{r=1}^{R}S_{nr}^{22}\eta_r\right)-\left(2\frac{\bar{f}}{\bar{\Omega}_0}+\frac{\bar{f}^2}{\bar{\Omega}_0^2}\right)\left(\sum_{r=1}^{R}Q_{nr}^{21}\zeta_r+\sum_{r=1}^{R}Q_{nr}^{22}\eta_r\right), \tag{29b}$$

where $S_{nl}^{ij}$ and $Q_{nl}^{ij}$ are the $i$–$j$th entries of the $n$–$l$th block matrices of $[S]$ and $[Q]$, and $\{u\}=[\varsigma_1,\eta_1,\varsigma_2,\eta_2,\ldots,\varsigma_R,\eta_R]$.

In this article, the perturbation velocity, $\bar{f}(t)$, is assumed to be very small and periodic. Therefore, it can be expressed as a Fourier series, i.e., $\bar{f}(t)=\sum_{j=-Q}^{Q}F_j e^{i\bar{\theta}_j t}$, where the parameter $\bar{\theta}_j$ is the perturbation frequency. As noted, the fluctuation term $\bar{f}(t)$ is so small in comparison to the constant speed $\bar{\Omega}_0$ that the module $F_j$ should also be much smaller than $\bar{\Omega}_0$. Consider a small parameter term $\varepsilon$ defined as $|F_M|/\bar{\Omega}_0$, where $|F_M|$ is the maximum magnitude of component $F_j$ for $j=1,2,3,\ldots,Q$. Then Eqs. (29a) and (29b) can be rewritten as

$$\dot{\varsigma}_n-\bar{\omega}_n\eta_n=-2\varepsilon\tilde{f}\left(\sum_{r=1}^{R}S_{nr}^{11}\zeta_r+\sum_{r=1}^{R}S_{nr}^{12}\eta_r\right)-\left(2\varepsilon\tilde{f}+\varepsilon^2\tilde{f}^2\right)\left(\sum_{r=1}^{R}Q_{nr}^{11}\zeta_r+\sum_{r=1}^{R}Q_{nr}^{12}\eta_r\right), \tag{30a}$$

$$\dot{\eta}_n+\bar{\omega}_n\varsigma_n=-2\varepsilon\tilde{f}\left(\sum_{r=1}^{R}S_{nr}^{21}\zeta_r+\sum_{r=1}^{R}S_{nr}^{22}\eta_r\right)-\left(2\varepsilon\tilde{f}+\varepsilon^2\tilde{f}^2\right)\left(\sum_{r=1}^{R}Q_{nr}^{21}\zeta_r+\sum_{r=1}^{R}Q_{nr}^{22}\eta_r\right), \tag{30b}$$

where $\tilde{f}=\bar{f}/|F_M|$.

By employing the multiple scales perturbation method [15], the solution for Eqs. (30a) and (30b) can then be expressed in terms as

$$u_n(t,\varepsilon)=u_{n0}(T_0,T_1,T_2,\ldots)+\varepsilon u_{n1}(T_0,T_1,T_2,\ldots)+\varepsilon^2u_{n2}(T_0,T_1,T_2,\ldots)+\cdots, \tag{31}$$

where $T_\alpha=\varepsilon^\alpha t$ for $\alpha=0,1,2,\ldots$.

Substitute Eq. (31) into Eqs. (30a) and (30b), leading to

Order $\varepsilon^0$

$$D_0\varsigma_{n0}-\bar{\omega}_n\eta_{n0}=0, \tag{32a}$$

$$D_0\eta_{n0}+\bar{\omega}_n\varsigma_{n0}=0. \tag{32b}$$

Order $\varepsilon^1$

$$D_0\varsigma_{n1} - \bar{\omega}_n\eta_{n1} = -D_1\varsigma_{n0} - 2\tilde{f}\left(\sum_{r=1}^{R} S_{nr}^{11}\zeta_{r0} + \sum_{r=1}^{R} S_{nr}^{12}\eta_{r0}\right) - 2\tilde{f}\left(\sum_{r=1}^{R} Q_{nr}^{11}\zeta_{r0} + \sum_{r=1}^{R} Q_{nr}^{12}\eta_{r0}\right), \tag{33a}$$

$$D_0\eta_{n1} + \bar{\omega}_n\varsigma_{n1} = -D_1\eta_{n0} - 2\tilde{f}\left(\sum_{r=1}^{R} S_{nr}^{21}\zeta_{r0} + \sum_{r=1}^{R} S_{nr}^{22}\eta_{r0}\right) - 2\tilde{f}\left(\sum_{r=1}^{R} Q_{nr}^{21}\zeta_{r0} + \sum_{l=1}^{R} Q_{nr}^{22}\eta_{r0}\right), \tag{33b}$$

where

$$\frac{\mathrm{d}}{\mathrm{d}t} = \frac{\mathrm{d}T_0}{\mathrm{d}t}\frac{\partial}{\partial T_0} + \frac{\mathrm{d}T_1}{\mathrm{d}t}\frac{\partial}{\partial T_1} + \frac{\mathrm{d}T_2}{\mathrm{d}t}\frac{\partial}{\partial T_2}\cdots = D_0 + \varepsilon D_1 + \varepsilon^2 D_2\cdots \tag{34}$$

and $\partial/\partial T_j = D_j$. Due to the complexity of this investigation and the small difference in the first- and second-order approximation results [17,18,20], the second-order expansion was not carried out in this study. Based on the first-order approximate solution, it yields

$$\varsigma_{n0} = A_n(T_1)\exp(\mathrm{i}\bar{\omega}_n T_0) + c.c., \tag{35a}$$

$$\eta_{n0} = \mathrm{i}A_n(T_1)\exp(\mathrm{i}\bar{\omega}_n T_0) + c.c., \tag{35b}$$

where $A_n(T_1)$ is an undetermined function of $T_1$, and the corresponding complex conjugate terms are denoted by *c.c.* Assuming that $\tilde{f}_0 = 0$ and $\tilde{f} = \sum_{j=1}^{Q}\hat{F}_k\mathrm{e}^{\mathrm{i}\bar{\theta}_j t} + c.c.$, and substituting the general solutions, i.e., Eqs. 35(a) and 35(b), into Eqs. 33(a) and 33(b), the following solutions can be derived:

$$\begin{aligned} D_0\varsigma_{n1} - \bar{\omega}_n\eta_{n1} = {} & D_1 A_n\mathrm{e}^{\mathrm{i}\bar{\omega}_n T_0} - 2\sum_{j=1}^{Q}\hat{F}_j\sum_{r=1}^{R} S_{nr}^{11}\left\{A_r\mathrm{e}^{\mathrm{i}[\bar{\theta}_j+\bar{\theta}_r]T_0} + \bar{A}_r\mathrm{e}^{\mathrm{i}[\bar{\theta}_j-\bar{\theta}_r]T_0}\right\} \\ & - 2\sum_{j=1}^{Q}\hat{F}_j\sum_{r=1}^{R} S_{nr}^{12}\left\{\mathrm{i}A_r\mathrm{e}^{\mathrm{i}[\bar{\theta}_j+\bar{\theta}_r]T_0} - \mathrm{i}\bar{A}_r\mathrm{e}^{\mathrm{i}[\bar{\theta}_j-\bar{\theta}_r]T_0}\right\} \\ & - 2\sum_{j=1}^{Q}\hat{F}_j\sum_{r=1}^{R} Q_{nr}^{11}\left\{A_r\mathrm{e}^{\mathrm{i}[\bar{\theta}_j+\bar{\theta}_r]T_0} + \bar{A}_r\mathrm{e}^{\mathrm{i}[\bar{\theta}_j-\bar{\theta}_r]T_0}\right\} \\ & - 2\sum_{j=1}^{Q}\hat{F}_j\sum_{r=1}^{R} Q_{nr}^{12}\left\{\mathrm{i}A_r e^{\mathrm{i}[\bar{\theta}_j+\bar{\theta}_r]T_0} - \mathrm{i}\bar{A}_r\mathrm{e}^{\mathrm{i}[\bar{\theta}_j-\bar{\theta}_r]T_0}\right\} + c.c., \end{aligned} \tag{36a}$$

$$\begin{aligned} D_0\eta_{n1} + \bar{\omega}_n\varsigma_{n1} = {} & -\mathrm{i}D_1 A_n\mathrm{e}^{\mathrm{i}\bar{\omega}_n T_0} - 2\sum_{j=1}^{Q}\hat{F}_j\sum_{r=1}^{R} S_{nr}^{21}\left\{A_r\mathrm{e}^{\mathrm{i}[\bar{\theta}_j+\bar{\theta}_r]T_0} + \bar{A}_r\mathrm{e}^{\mathrm{i}[\bar{\theta}_j-\bar{\theta}_r]T_0}\right\} \\ & - 2\sum_{j=1}^{Q}\hat{F}_j\sum_{r=1}^{R} S_{nr}^{22}\left\{\mathrm{i}A_r\mathrm{e}^{\mathrm{i}[\bar{\theta}_j+\bar{\theta}_r]T_0} - \mathrm{i}\bar{A}_r\mathrm{e}^{\mathrm{i}[\bar{\theta}_j-\bar{\theta}_r]T_0}\right\} \\ & - 2\sum_{j=1}^{Q}\hat{F}_j\sum_{r=1}^{R} Q_{nr}^{21}\left\{A_r\mathrm{e}^{\mathrm{i}[\bar{\theta}_j+\bar{\theta}_r]T_0} + \bar{A}_r\mathrm{e}^{\mathrm{i}[\bar{\theta}_j-\bar{\theta}_r]T_0}\right\} \\ & - 2\sum_{j=1}^{Q}\hat{F}_j\sum_{r=1}^{R} Q_{nr}^{22}\left\{\mathrm{i}A_r\mathrm{e}^{\mathrm{i}[\bar{\theta}_j+\bar{\theta}_r]T_0} - \mathrm{i}\bar{A}_r\mathrm{e}^{\mathrm{i}[\bar{\theta}_j-\bar{\theta}_r]T_0}\right\} + c.c., \end{aligned} \tag{36b}$$

where, $\bar{A}_r$ denotes the complex conjugate of $A_r$. This choice depends upon the resonant combinations of the frequencies. Three different cases were considered herein. All of the resonant combination cases will be studied as follows.

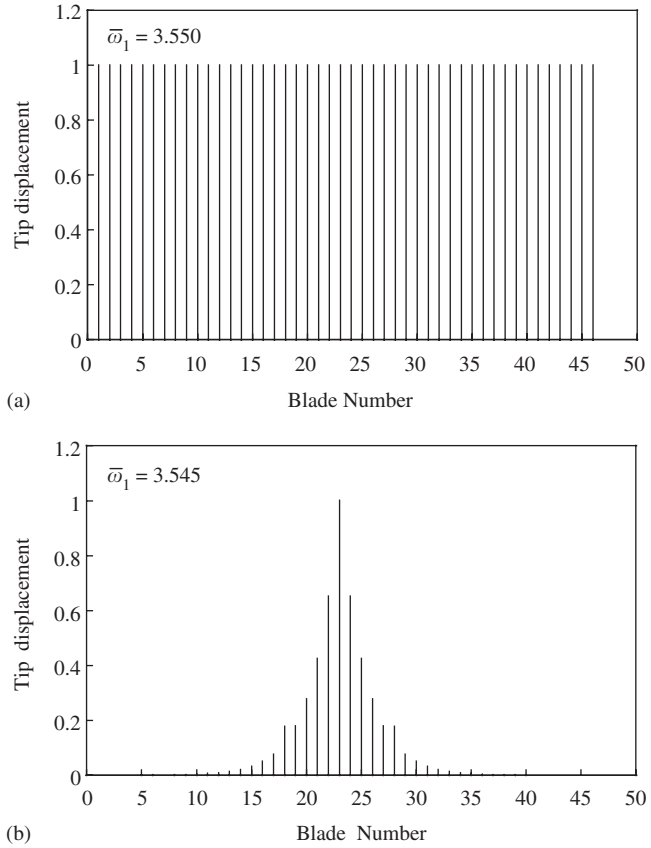


Fig. 2. Tip displacement patterns of a cracked blade-disk system at the lowest natural frequency. (with $\bar{\beta} = 0.05$, $\bar{R}_c = 1.0$, $\bar{\Omega}_0 = 0.5$): (a) without a crack, $\bar{\gamma} = 0.0$; (b) with a crack, $\bar{\gamma} = 0.025$.

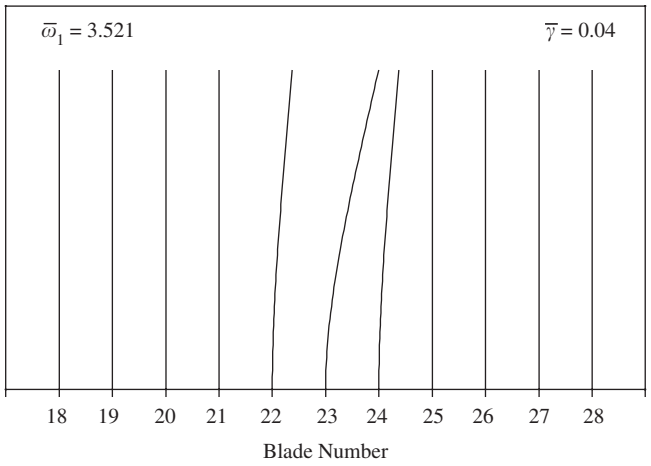


Fig. 3. The localization mode shape of a cracked blade-disk system ($\bar{\beta} = 0.05$, $\bar{R}_c = 1.0$, $\bar{\Omega}_0 = 0.5$).

(i) the frequency $\bar{\theta}_j$ is away from $\bar{\omega}_p \pm \bar{\omega}_q$

The existence of the term $e^{i\bar{\omega}_n T_0}$ in the general solutions for Eqs. 36(a), and 36(b) may make it difficult to find the particular solutions. For simplicity, the corresponding particular solutions are assumed as

$$\varsigma_{n1} = B_{n1}(T_1)e^{i\bar{\omega}_n T_0} + c.c., \tag{37a}$$

$$\eta_{n1} = B_{n2}(T_1)e^{i\bar{\omega}_n T_0} + c.c., \tag{37b}$$

where $B_{n1}$ and $B_{n2}$ are the coefficients to be determined. Substituting the above equations into Eqs. 36(a) and 36(b), it leads to

$$i\bar{\omega}_n B_{n1} - \bar{\omega}_n B_{n2} = -D_1 A_n, \tag{38a}$$

$$\bar{\omega}_n B_{n1} + i\bar{\omega}_n B_{n2} = -iD_1 A_n. \tag{38b}$$

The coefficients of $B_{n1}$ and $B_{n2}$ can be solved, if and only if the following equation can be satisfied:

$$\begin{vmatrix} i\bar{\omega}_n & -D_1 A_n \\ \bar{\omega}_n & -iD_1 A_n \end{vmatrix} = 0. \tag{39}$$

Eq. (39) yields the results, in which $D_1 A_n$ must be null. In other words, the value of $A_n(T_1)$ should be a constant. Hence, the system would be always stable in this state.

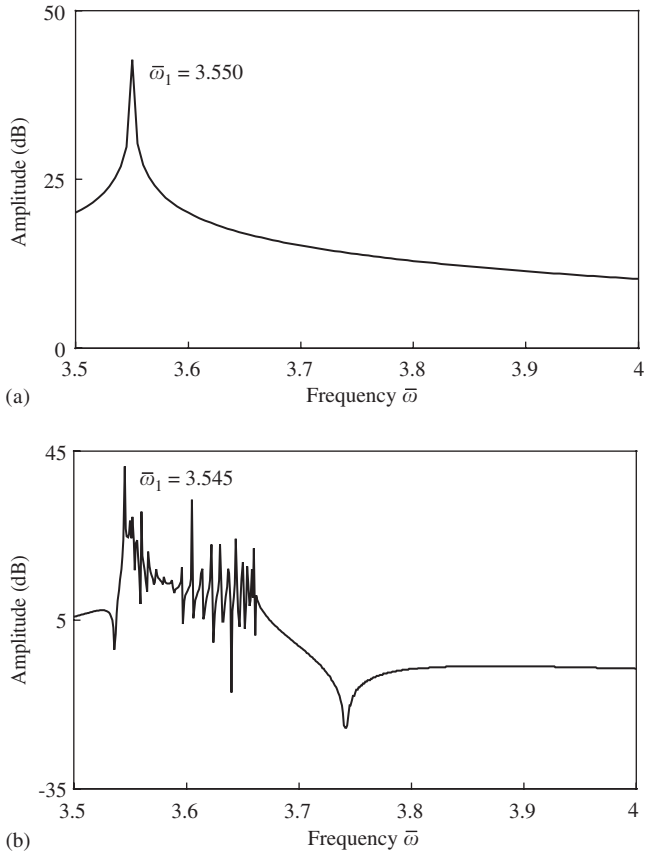


Fig. 4. Tip frequency responses at the tip of the 23th blade (with $\bar{\beta} = 0.05$, $\bar{R}_c = 1.0$, $\bar{\Omega}_0 = 0.5$): (a) without a crack, $\bar{\gamma} = 0.0$; (b) with a crack, $\bar{\gamma} = 0.025$.

(ii) the frequency $\bar{\theta}_j$ near to $\bar{\omega}_p + \bar{\omega}_q$

The transition curves were used to mark the boundaries between the stable and the unstable zones. In this case, the transition curves are

$$\bar{\theta}_j = \bar{\omega}_p + \bar{\omega}_q \pm 2\varepsilon\sqrt{\Lambda_{pq}\bar{\Lambda}_{qp}} + O(\varepsilon^2), \tag{40}$$

where

$$\Lambda_{pq} = \hat{F}_j\left(-\mathrm{i}S_{pq}^{21} - S_{pq}^{22} - \mathrm{i}Q_{pq}^{21} - Q_{pq}^{22}\right) - \hat{F}_j\left(-S_{pq}^{11} + \mathrm{i}S_{pq}^{12} - Q_{pq}^{11} + \mathrm{i}Q_{pq}^{12}\right), \tag{41a}$$

$$\Lambda_{qp} = \hat{F}_j\left(-\mathrm{i}S_{qp}^{21} - S_{qp}^{22} - \mathrm{i}Q_{qp}^{21} - Q_{qp}^{22}\right) - \hat{F}_j\left(-S_{qp}^{11} + \mathrm{i}S_{qp}^{12} - Q_{qp}^{11} + \mathrm{i}Q_{qp}^{12}\right). \tag{41b}$$

(iii) the frequency $\bar{\theta}_j$ near to $\bar{\omega}_p - \bar{\omega}_q$

Similarly, the different types of combination resonance transition curves can be solved from

$$\bar{\theta}_j = \bar{\omega}_p - \bar{\omega}_q \pm 2\varepsilon\sqrt{\Lambda_{pq}\Lambda_{qp}} + O(\varepsilon^2). \tag{42}$$

## 4. Numerical results and discussions

As noted in many papers [14], a local crack in a periodically shrouded blade may not only alter the local stiffness of this blade, but may also introduce the so-called mode localization phenomenon. Theoretically, the

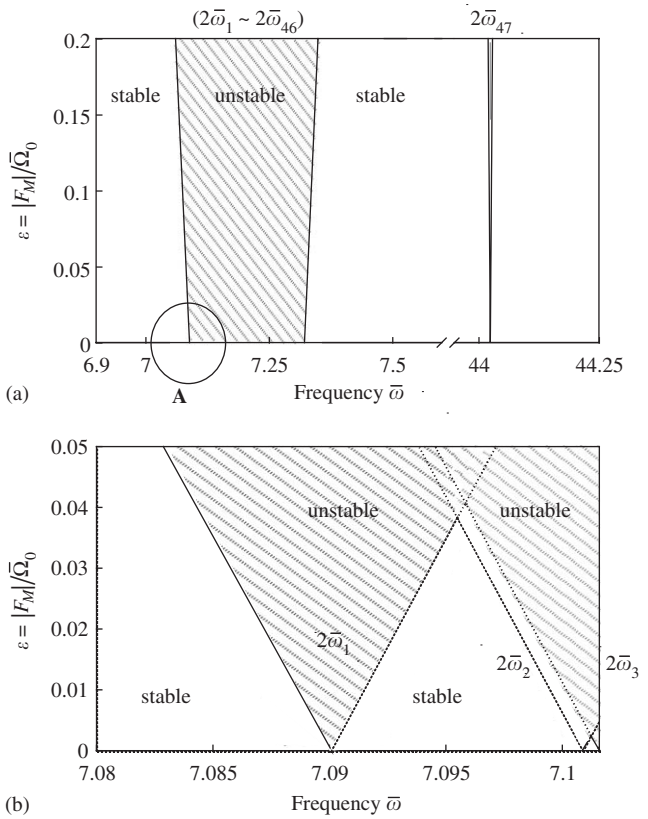


Fig. 5. Stability transition curves for the cracked blade-disk system (with $\bar{\beta} = 0.05$, $\bar{R}_c = 1.0$, $\bar{\Omega}_0 = 0.5$, $\bar{\gamma} = 0.025$): (a) the regions of instability; (b) the detail of zone $A$.

mode localization phenomenon will confine the energy of the fluctuating vibration to just a few blades near the cracked blade at the localization frequency. The interaction between the crack size and mode localization speeds up the crack propagation and enhance the localization. To investigate the possible effect of the mode localization phenomenon on the dynamic instability zones in a mistuned periodical system, a shrouded blade disk with 46 blades attached to a rigid hub was simulated numerically. A near root crack on the 23rd blade was assumed in this mistuned blade-disk system. The shape parameters of blades were: $(R_h/L) = 0.5$, $(b/L) = 0.227$, $(t/L) = 0.08$, and $\bar{r}^* = 0$. The effects of rotation speed, crack size and shroud stiffness on the stability zone variations were studied. For simplicity, the perturbation speed was assumed to be $\bar{f}(t) = 2\cos\bar{\omega}t$.

For the sake to study mode localization, a number of apparently identical blades are distributed periodically around a rigid hub. In other words, the effect of disk flexibility is ignored in this study. Similar models have been employed in Refs. [3–5,14]. Based on the rigid hub assumption, the zero nodal diameter mode is not included in this paper. The mode localization effect on the lowest mode is illustrated in Fig. 2. Fig. 2(a) shows the blade tip displacement pattern in this blade-disk system without any crack, i.e., $\bar{\gamma} = 0$. A uniform tip displacement was found for the lowest mode. The blade tip displacement pattern of the system with a crack $\bar{\gamma} = 0.025$ in size is shown in Fig. 2(b). Fig. 3 displays the corresponding mode shape for this localization mode. The blade tip displacement pattern or the mode shape shows modal localization in this mistuned system. The vibration energy will be confined to just a few blades that are near the cracked blade, i.e., the 23rd blade. Fig. 4 shows the difference in frequency responses for the tuned and mistuned systems at the tip of the 23rd blade. Due to the repeated frequencies, $\bar{\omega}_1 = \bar{\omega}_2 = \cdots = \bar{\omega}_{46} = 3.550$, of the periodic system, only a single peak at $\bar{\omega}_1 = 3.550$ is observed for the tuned system, i.e., a system without any cracks. Contrary to the single peak in the tuned system, a quite complicated frequency spectrum distribution, as shown in Fig. 4(b), was found in the system if a local crack near

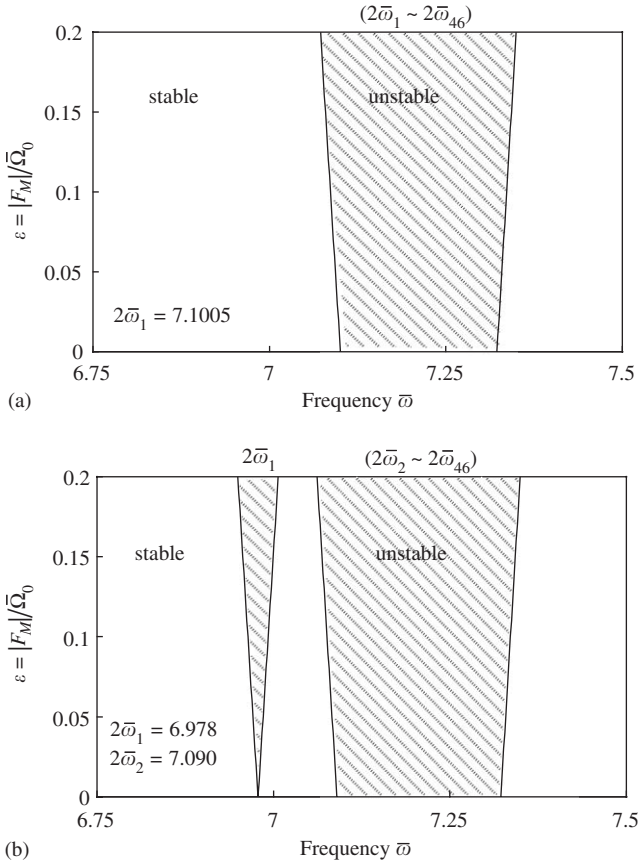


Fig. 6. The variations in stability on the cracked system with different crack sizes (with $\bar{\beta} = 0.05$, $\bar{R}_c = 1.0$, $\bar{\Omega}_0 = 0.5$): (a) without a local crack; (b) with a crack of size $\bar{\gamma} = 0.05$.

the blade root existed. Multiple peaks are found near the lowest frequency, i.e., the localization frequency $\bar{\omega}_1 = 3.545$. Fig. 5(a) shows the unstable zone distribution in the mistuned system. Results indicated that a wide unstable region, i.e., $2\bar{\omega} = 7.09-7.33$, was grouped by a bundle of 46 very close unstable zones. These individual unstable zones arise from a bond of local frequencies $\bar{\omega}_1, \ldots, \bar{\omega}_{46}$. Fig. 5(b) shows the details of these closely distributed individual unstable zones. This grouped unstable zone is related to the spread of the frequencies as shown in Fig. 4(b). The localization phenomenon introduced by the local crack split the 46 identical lowest frequencies of a periodically arranged shrouded blade system into a series of 46 closely distributed frequencies. These closely distributed unstable regions were grouped and made a wide unstable band. In other words, the modal localization arising from a local blade crack might expand the unstable region near the local mode frequency.

The dynamic stability in a cracked shrouded blade-disk system may be affected by different parameters, i.e., the crack size, rotation speed and the shroud stiffness. The effect of local crack on the dynamic stability in this shrouded system is shown in Figs. 6(a) and (b). A grouped unstable zone, as shown in Fig. 6(a), was found for the blade-disk system without a crack, i.e., $\bar{\gamma} = 0.0$. The lowest natural frequency, i.e., the so-called localization frequency, will shift from $2\bar{\omega}_1 = 7.1005$ to a lower frequency value $2\bar{\omega}_1 = 6.978$ as the crack size is propagated from $\bar{\gamma} = 0.0$ to 0.050. Results in Fig. 6(b) show that an additional unstable band near the localization frequency is introduced due to the existence of the local crack. The unstable zone, as shown in Fig. 6(b), is enlarged as the crack size is increased. Hence, it can be concluded that the local crack enlarges the unstable zone and shift it toward a lower frequency region. Figs. 7(a) and (b) show the variation in the dynamic stability as the rotation speed is increased from $\bar{\Omega}_0 = 0.25$ to 5.0. Results indicated that the unstable band is enlarged and shifts to a higher frequency region as the rotation speed $\bar{\Omega}_0$ is increased.

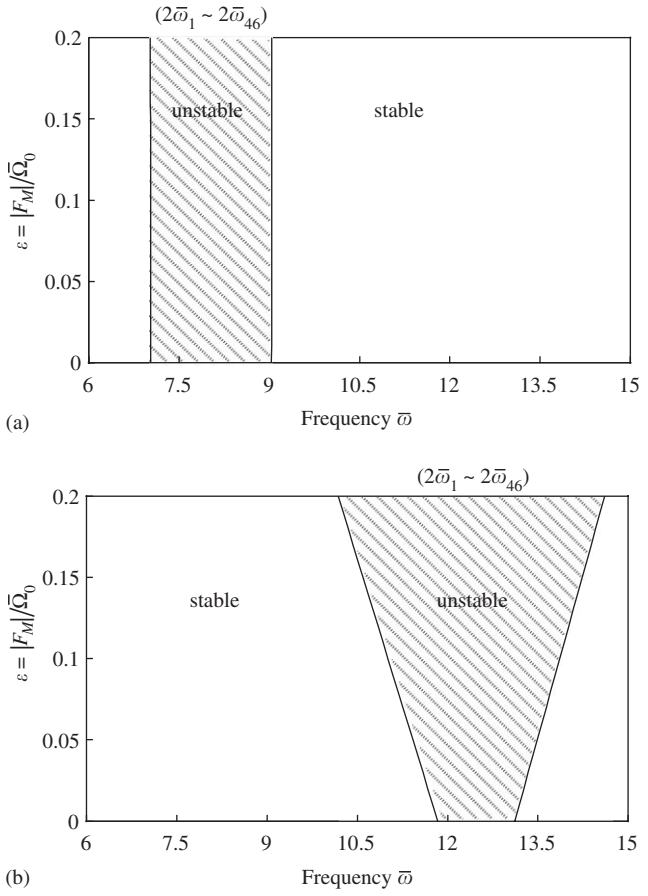


Fig. 7. The variations in stability on the cracked system under different rotation speeds (with $\bar{\beta} = 0.05$, $\bar{R}_c = 1.0$, $\bar{\gamma} = 0.05$): (a) at a speed of $\bar{\Omega}_0 = 0.25$; (b) at a speed of $\bar{\Omega}_0 = 5.0$.

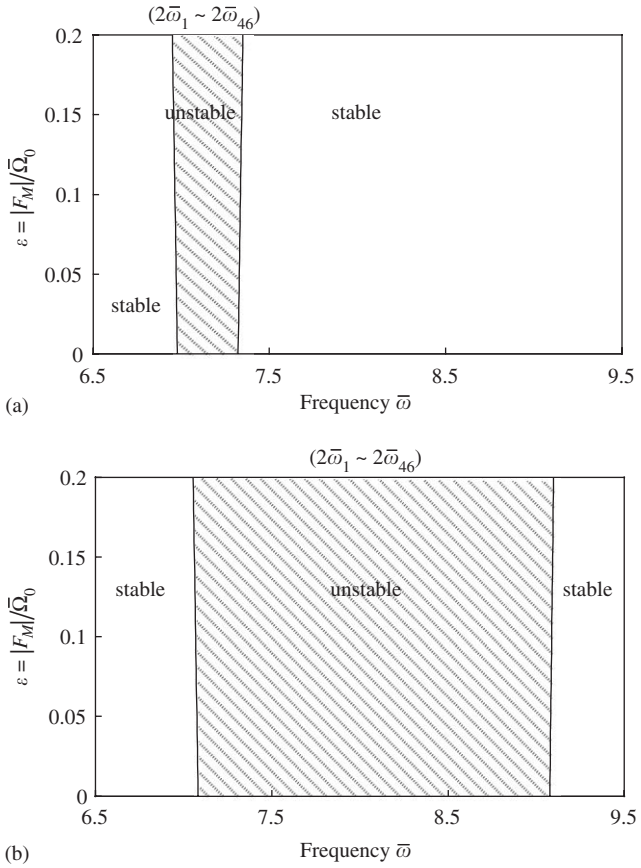


Fig. 8. The variations in stability on the cracked system with various shroud coupling stiffness (with $\bar{R}_c = 1.0$, $\bar{\Omega}_0 = 0.5$, $\bar{\gamma} = 0.05$): (a) with a stiffness of $\bar{\beta} = 0.05$; (b) with a stiffness of $\bar{\beta} = 0.5$.

As noted by a number of investigators [4,5], the degree of localization depends significantly upon the magnitude of the disorder and coupling stiffness. In a mistuned blade-disk system, the shroud stiffness is considered as the coupling stiffness. The stability zones in this mistuned blade-disk system with various shroud stiffness, $\bar{\beta} = 0.05$ and 0.5, are plotted in Figs. 8(a) and (b). The calculated results indicated that the effect of the shroud stiffness in this periodic system is also one of the most sensitive parameters. Excluding the localization frequency $\bar{\omega}_1$, the other natural frequencies $\bar{\omega}_2 - \bar{\omega}_{46}$ will increase and spread out as the coupling stiffness is increased. The unstable band would swell as the coupling stiffness is increased.

Fig. 9 displays the variations in dynamic stability for the mistuned blade-disk system with and without considering the Coriolis effect. These results indicate that the first unstable zone near $2\bar{\omega}_1$ may shift to a lower frequency as the Coriolis effect is considered.

## 5. Conclusions

The localization mode effect on the stability in a rotational blade disk with a cracked blade was investigated. Simulated results indicated that the local crack may not only confine the disturbed energy in the blades to those near the cracked blade but also may change the instability range of the disordered blade disk significantly. The major conclusions that can be drawn from this study, are given as

(1) The crack depth is one of the most important parameters for stability in a rotating mistuned blade-disk system. The shift in localization frequency will enlarge the total unstable zone near the frequency $2\bar{\omega}_1$ as the depth of the crack increases.

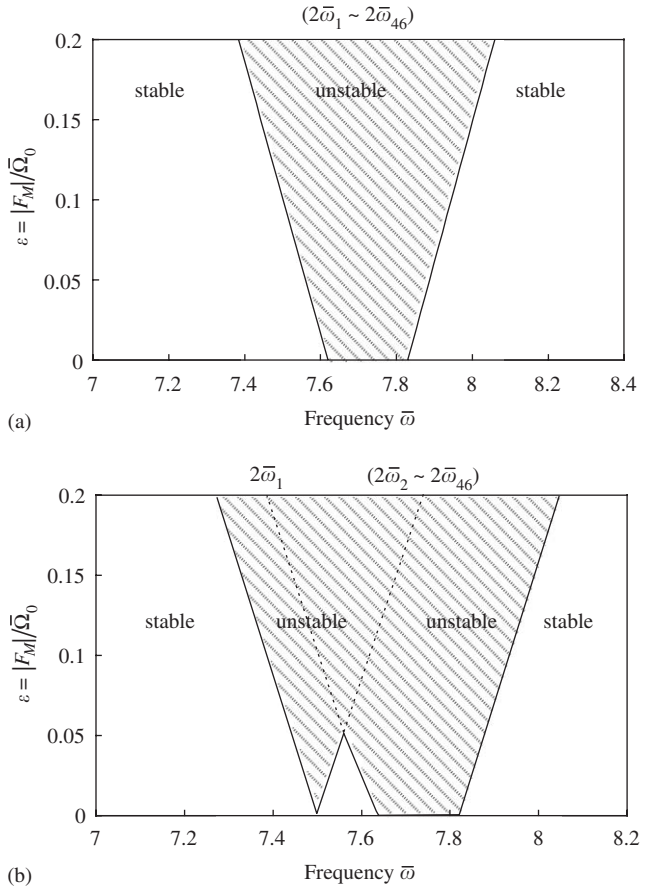


Fig. 9. The stability zones for a cracked blade-disk system with and without considering the Coriolis effect (with $\bar{\beta} = 0.05$, $\bar{R}_c = 1.0$, $\bar{\Omega}_0 = 0.5$, $\bar{\gamma} = 0.05$): (a) without Coriolis effect; (b) with Coriolis effect.

(2) The rotational speed may also change the instability zone in the mistuned system. It is observed that the unstable band $(2\bar{\omega}_1 - 2\bar{\omega}_{46})$ will expand and shift towards a higher frequency range as the rotational speed increases.
(3) Simulated results indicate that the instability band will swell as the shroud stiffness increases in a mistuned blade-disk system.

## Acknowledgment

This material is based upon work supported by the National Science Council of ROC under Grant NSC93-ET-7-110-004-ET to the National Sun Yat-Sen University.

## References

[1] O.O. Bendiksen, Mode localization phenomena in large space structures, *AIAA Journal* 25 (1987) 1241–1248.
[2] C.H. Hodges, Confinement of vibration by structural irregularity, *Journal of Sound and Vibration* 82 (1982) 411–424.
[3] C. Pierre, E.H. Dowell, Localization of vibrations by structural irregularity, *Journal of Sound and Vibration* 114 (1987) 549–564.
[4] S.T. We, C. Pierre, Localization phenomena in moistened assemblies with cyclic symmetry part I: free vibrations, *Transactions of ASME, Journal of Vibration, Acoustics, Stress, and Reliability in Design* 110 (1988) 429–438.

[5] S.T. We, C. Pierre, Localization phenomena in mistuned assemblies with cyclic symmetry part ii: forced vibrations, *Transactions of ASME, Journal of Vibration, Acoustics, Stress, and Reliability in Design* 110 (1988) 439–449.
[6] C.W. Cai, Y.K. Cheung, H.C. Chen, Mode localization phenomena in nearly periodic systems, *Transactions of ASME, Journal of Applied Mechanics* 62 (1995) 141–149.
[7] C.W. Cai, H.C. Chen, Y.K. Cheung, Localization modes in periodic systems with nonlinear disorders, *Transactions of the ASME, Journal of Applied Mechanics* 64 (1997) 940–945.
[8] D.J. Cottney, D.J. Ewins, Towards the efficient vibration analysis of shrouded bladed disk assemblies, *Transactions of ASME, Journal of Engineering for Industry* 96B (1974) 1054–1059.
[9] H.L. Bernstein, J.M. Allen, Analysis of cracked gas turbine blades, *Transactions of ASME, Journal of Engineering for Gas Turbines and Power* 114 (1992) 293–301.
[10] D.P. Walls, R.E.S.E. deLaneuville, Cunningham, damage tolerance based life prediction in gas turbine engine blades under vibratory high cycle fatigue, *Transactions of ASME, Journal of Engineering for Gas Turbines and Power* 119 (1997) 143–146.
[11] D. Afolabi, The frequency response of mistuned bladed disk assemblies, in: *Proceedings of the Tenth Biennial Conference on Mechanical Vibration and Noise*, Cincinnati, Ohio, USA. The Frequency Response of Mistuned Bladed Disk Assemblies, 1985.
[12] D. Afolabi, The eigenvalue spectrum of mistuned bladed disk, in: *Proceedings of the Tenth Biennial Conference on Mechanical Vibration and Noise*, Cincinnati, Ohio, USA, 1985.
[13] P. Basu, J.H. Griffin, The effect of limiting aerodynamic and structural coupling in models of mistuned blade disk vibration, in: *Proceedings of the Tenth Biennial Conference on Mechanical Vibration and Noise*, Cincinnati, Ohio, USA, 1985.
[14] J.H. Kuang, B.W. Huang, Modal localization of a cracked bladed disk, *Transactions of ASME, Journal of Engineering for Gas Turbine and Power* 121 (2) (1999) 335–342.
[15] A.H. Nayfey, D.T. Mook, Parametric excitations of linear systems having many degrees of freedom, *Journal of the Acoustical Society of America* 62 (2) (1977) 375–381.
[16] C.S. Hsu, On a restricted class of coupled hill's equations and some applications, *Transactions of ASME, Journal of Applied Mechanics* (1961) 551–557.
[17] T.H. Young, Dynamic response of a pretwisted, tapered beam with non-constant rotating speed, *Journal of Sound and Vibration* 150 (3) (1991) 435–446.
[18] C.L. Liao, B.W. Huang, Parametric resonance of a spinning pretwisted beam with time-dependent spinning rate, *Journal of Sound and Vibration* 180 (1) (1995) 47–65.
[19] O.O. Bendiksen, Flutter of mistuned turbo machinery rotors, *Transactions of ASME, Journal of Engineering for Gas Turbines and Power* 106 (1984) 25–33.
[20] T.H. Young, G.T. Liou, Coriolis effect on the vibration of a cantilever plate with time-varying rotating speed, *Transactions of ASME, Journal of Vibration and Acoustics* 114 (1992) 232–241.
[21] K.B. Subrahmanyam, K.R.V. Kaza, Vibration and buckling of rotating, pretwisted, preconed beams including corilis effects, *Transactions of ASME, Journal of Vibration, Acoustics, Stress, and Reliability in Design* 108 (1986) 140–149.
[22] B.W. Huang, J.H. Kuang, Mode localization in a rotating mistuned turbo disk with Coriolis effect, *International Journal of Mechanical Science* 43 (2001) 1643–1660.
[23] G.L. Anderson, On the extensional and flexural vibrations of rotating bar, *International Journal of Nonlinear Mechanics* 10 (1975) 223–236.
[24] C.A. Papadopoulos, A.D. Dimarogonas, Coupled longitudinal and bending vibrations of a crack shaft, *Transactions of ASME, Journal of Vibration, Acoustics, Stress, and Reliability in Design* 110 (1988) 1–8.
[25] D. Broek, *Elementary Engineering Fracture Mechanics*, Martinus Nijhoff Publishers, Dordrecht, 1986.
[26] H. Tada, P. Paris, G. Irwin, The Stress Analysis of Crack Handbook, Vol. 2.13–2.14, Del Research Corporation, Hellertown, Pennsylvania, 1973.
[27] L. Chen, C. Chen, Vibration and stability of cracked thick rotating blade, *Computers & Structures* 28 (1) (1988) 67–74.
[28] B. Grabowski, The vibrational behavior of a turbine rotor containing a transverse crack, *Transactions of ASME, Journal of Mechanic Design* 102 (1980) 140–146.
[29] M.C. Wu, S.C. Huang, On the vibration of a cracked rotating blade, *Shock and Vibration* 5 (5–6) (1998) 317–323.
[30] M.H.H. Shen, C. Pierre, Free-vibrations of beams with a single-edge crack, *Journal of Sound and Vibration* 170 (2) (1994) 237–259.
[31] T.Y. Ng, K.Y. Lam, H. Li, Dynamic stability of rotating blades with transverse cracks, *Shock and Vibration* 10 (3) (2003) 187–194.
[32] C.Y. Lin, L.W. Chen, Dynamic stability of rotating pre-twisted blades with a constrained damping layer, *Composite Structures* 61 (3) (2003) 235–245.
[33] G. Sakar, M. Sabuncu, Dynamic stability of a rotating asymmetric cross-section blade subjected to an axial periodic force, *International Journal of Mechanical Sciences* 45 (9) (2003) 1467–1482.
[34] G. Sakar, S. Mustafa, Buckling and dynamic stability of a rotating pretwisted asymmetric cross-section blade subjected to an axial periodic force, *Finite Elements in Analysis and Design* 40 (11) (2004) 1399–1415.